Computation of window quantities in $a_\mu^{\text{LO-HVP}}$

Bálint C. Tóth[a,b] for the Budapest–Marseille–Wuppertal collaboration

[a] Department of Physics, University of Wuppertal, Gaussstrasse 20, D-42119, Germany
[b] Jülich Supercomputing Centre, Forschungszentrum Jülich, D-52425 Jülich, Germany

Window observables

We are computing several window observables to $a_\mu^{\text{LO-HVP}}$. They are obtained through a weighted integral of the one-photon-irreducible, two-point function $G_{1\gamma\text{I}}(t)$ of the quark electromagnetic current:

$$a_{\mu,t_0-t_1}^{\text{LO-HVP}} = \alpha^2 \int_0^\infty dt\, K(tm_\mu)\, W_{t_0-t_1}(t)\, G_{1\gamma\text{I}}(t) ,$$

where $K(tm_\mu)$ is a known kinematic function [1–4], and $W_{t_0-t_1}(t)$ is the smooth window function [5] restricting the integral within the Euclidean time range between t_0 and t_1. We focus on $a_{\mu,04-10}^{\text{LO-HVP}}$ and $a_{\mu,28-\infty}^{\text{LO-HVP}}$ [6], the windows extending respectively from 0.4 fm to 1.0 fm, and from 2.8 fm to infinity.

Continuum extrapolation

We perform global fits to the lattice spacing and quark mass dependence.

Lattice spacing dependence. The naive a^2-like behaviour is modified to $\alpha_s^n a^2$ by anomalous dimensions of operators in the Symanzik effective theory [8], where α_s is the strong coupling at the scale of the lattice spacing. To account for this uncertainty, we use two types of fits:

- $A(a^2)$: Conventional polynomial in a^2/w_0^2.
- $A'(\Delta_{KS})$: Scaling of staggered taste violation parameter Δ_{KS} is compatible to $\alpha_s^n a^2$ with $n = 3$ $\longrightarrow$ use polynomials of $\Delta_{KS} w_0^2$.

Quark mass dependence. The deviation from the physical light and strange quark mass is described by the variables

$$X_l = \hat{M}^2 w_0^2 - \left[\hat{M}^2 w_0^2\right]_{\text{phys}} \quad \text{and} \quad X_s = M_{ss}^2 w_0^2 - \left[M_{ss}^2 w_0^2\right]_{\text{phys}} ,$$

where $\hat{M}^2 = \frac{1}{2}\left(M_{uu}^2 + M_{dd}^2\right)$ and "phys" denotes the physical values taken from [7].

Putting together, the global fit function is

$$Y = A(a^2) + A'(\Delta_{KS}) + B(a^2)X_l + C(a^2)X_s ,$$

where Y is one of our dimensionless target observables. In the fit function we have the variations:

- A and A': Two scenarios:
  Either A can be linear, quadratic or cubic in a^2 and A' is set to zero,
  or A' can be linear, quadratic or cubic in Δ_{KS} and A is set to zero.
- B and C: both constant and linear polynomials in a^2.
- Omit between zero and four of the coarsest lattice spacings (out of a total of seven) from the fits. Include at least one more lattice spacings than number of coefficients in A or A', and two more than in B or C.

Distribution of observables

AIC/flat weights. For a given observable, to systematics related to the fit function and lattice spacing cuts we assign a weight using the Akaike Information Criterion (AIC) in a modified version as derived in Ref. [7]:

$$w = \exp\left[-\frac{1}{2}\left(\chi^2 + 2n_{\text{par}} - n_{\text{data}}\right)\right] ,$$

where n_{par} is the number of parameters in the fit, and the number of data points n_{data} accounts for the inclusion of different numbers of lattice spacings. Other systematics are assigned with flat weighting. From these inputs we construct a probability distribution function (PDF) for the observable Y

$$\text{PDF}(Y) = \sum_{i,a} \frac{w_{ia} \cdot \mathcal{N}(y_{ia}, \sigma_{ia}; Y)}{\sum_b w_{ib} \cdot \sum_j 1} ,$$

which includes both statistical and systematic variations. The weight w_{ia} corresponds to a systematics variation, whose flat weighted component is labelled by i, while its AIC weighted component is labelled by a. The statistical variations are assumed to follow a normal distribution, i.e. $\mathcal{N}(y, \sigma; Y)$ is a normal PDF with mean y and standard deviation σ.

Central value and error. The central value of Y is defined by the median of the constructed PDF. The lower and upper total errors are defined by quantiles of the corresponding cumulative distribution function (CDF)

- Standard 1σ: 15.87 % and 84.13 %.
- Half of standard 2σ: 2.28 % and 97.72 %.

Conservative estimate: take larger of these.

Combining distributions. In order to obtain the physical value of an observable Y, the physical values of w_0 and M_{ss} are included as inputs using the procedure[a]:

1. First we perform the analysis for Y at two fixed values of w_0 and two fixed values of M_{ss}, given by the edges of the central one-sigma bands of their distributions: Y_k with $k = 1, \ldots 4$.
2. Take a random selection for the systematic ingredients shared by Y, w_0 and M_{ss}.
3. Make a random selection for the remaining independent ingredients with a probability given by
$$P(i, a) = \frac{w_{ia}}{\sum_b w_{ib} \sum_j 1} ,$$
independently for w_0 and M_{ss}.
4. Perform a bilinear interpolation of the fit values and their corresponding χ^2 values from the Y_k obtained at fixed values of w_0 and M_{ss} to the sampled values.
5. Compute the weights corresponding to the interpolated χ^2 values and perform the above importance-sampling once more to obtain the desired sample Y^r.

After repeating the above procedure $N_R = 10^6$ times, we obtain the distribution of Y with the uncertainties of the physical values of w_0 and M_{ss} included.

[a] A similar sampling technique was recently proposed in Ref. [9].

Long-distance contributions

Although the vast majority of our final result (over 95%) comes directly from lattice simulations, we replaced the lattice calculation of the contribution to a_μ from $G(t)$ above $t \geq 2.8$ fm by a state-of-the-art, data-driven determination.

- As shown in the following Figure, the determinations of $a_{\mu,28-\infty}$ obtained using the $\pi^+\pi^-$ spectra measured by BaBar, KLOE, CMD-3 and in τ decays, are entirely consistent. The reason is that the tail contribution is dominated by the low-mass part of the spectrum, below the ρ peak, where all four measurements are in good agreement.

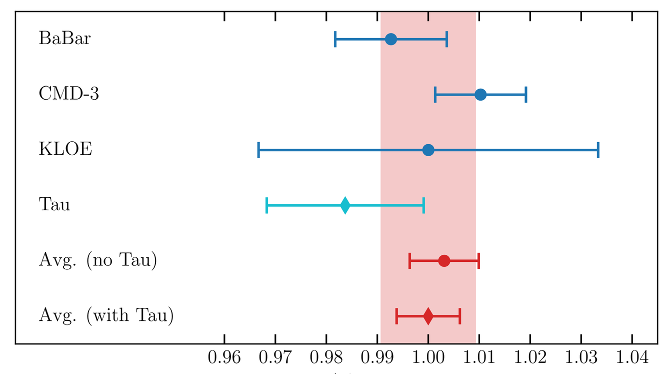

- We have checked that the data-driven contribution to a_μ from $t \geq 2.8$ fm is entirely compatible with our lattice calculation.

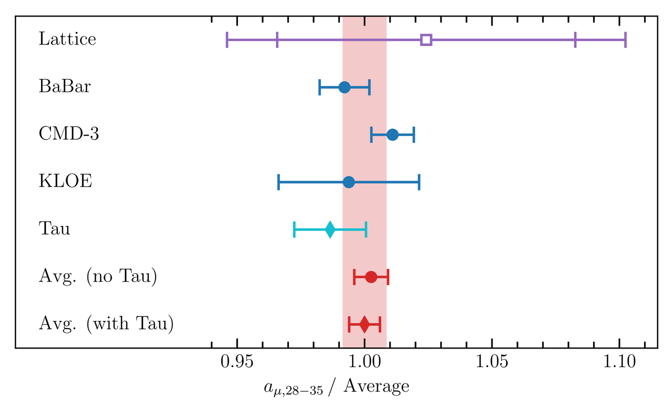

- The total uncertainty on our average of the data-driven $a_{\mu,28-\infty}$ is 0.26 in our 10^{-10} units, a number that must be compared to our total uncertainty of 3.3 on a_μ. Thus its impact on the uncertainty of our final result for a_μ is completely negligible.

Reasons for the choice of $t_{\text{cut}} = 2.8$ fm:

- Choosing to start the data-driven tail above $t = 2.8$ fm guarantees that the lattice contribution accounts for over 95% of our result for a_μ.
- Beyond reducing the uncertainty on $a_{\mu,28-\infty}$ by an order of magnitude, the use of a data-driven tail reduces the finite-volume correction that must be applied to the lattice result by a factor of 2 and the associated uncertainty by even more.
- For these large times the data-driven determinations of $a_{\mu,28-\infty}$ agree very well.

The computation is performed following the approach of Ref. [18]. The measurements of the $\pi^+\pi^-$ spectrum by BaBar [19, 20], KLOE [21–24], CMD-3 [25] and via hadronic τ decays [26, 27] are considered separately. Outside their center-of-mass energy ranges and for other hadronic channels, the data from each experiment are complemented by the combined experimental and perturbative QCD results compiled in Ref. [27, 28], with a full treatment of uncertainties and correlations. Then the HVPTools framework [28–31] is used to Laplace transform these four spectra into the corresponding Euclidean-time correlators, which are subsequently integrated to give the four data-driven results for $a_{\mu,28-\infty}$.
Altogether, we obtain

$$a_{\mu,28-\infty} = 27.59(17)(9)[26] \quad \text{and} \quad a_{\mu,28-35} = 18.12(11)(5)[16]$$

for our tail-related window results in the data-driven approach. The first error comes from the weighted average procedure of different experiments and includes a PDG-style error rescaling. The second error is the additional uncertainty from including or not including the τ data set. The third, conservative total error is the first two added linearly.

Intermediate window

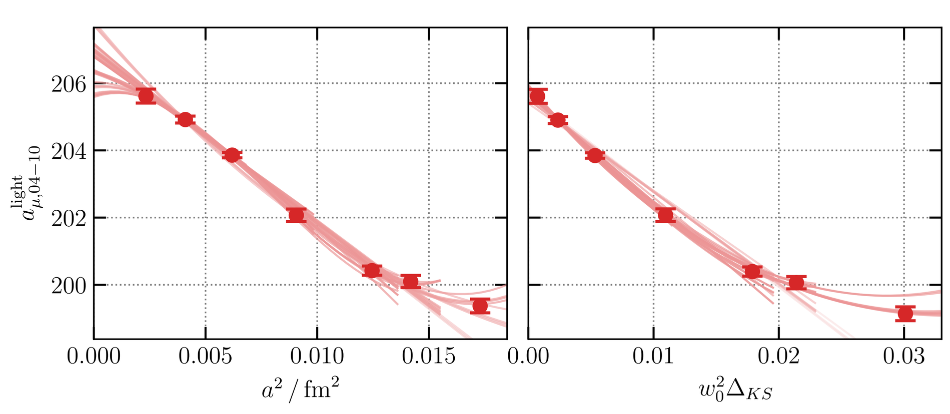

Figure 1: Representative continuum extrapolations of the intermediate window between 0.4 fm and 1.0 fm, as a function of a^2 (left), and Δ_{KS} (right). The data points are shifted to the physical point using the B and C coefficients.

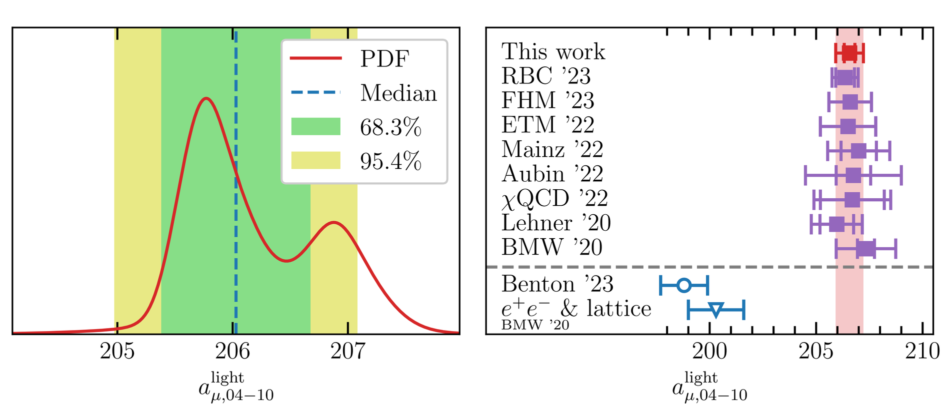

Figure 2: *Left:* PDF including both statistical and systematic variations. The median is given by the blue vertical line, the $1\sigma/2\sigma$ error band is shown with green/yellow color. *Right:* A comparison with other lattice results in the literature [7, 10–16], and a recent pure data-driven computation from Benton et al [17].

References

[1] B. e. Lautrup, A. Peterman and E. de Rafael, Phys. Rept. **3** (1972), 193-259
[2] E. de Rafael, Phys. Lett. B **322** (1994), 239-246 [arXiv:hep-ph/9311316].
[3] T. Blum, Phys. Rev. Lett. **91** (2003), 052001 [arXiv:hep-lat/0212018].
[4] D. Bernecker and H. B. Meyer, Eur. Phys. J. A **47** (2011), 148 [arXiv:1107.4388].
[5] T. Blum *et al.* [RBC and UKQCD], Phys. Rev. Lett. **121** (2018) no.2, 022003 [arXiv:1801.07224].
[6] A. Boccaletti, S. Borsanyi, *et al.* [arXiv:2407.10913].
[7] S. Borsanyi, Z. Fodor, *et al.* Nature **593** (2021) no.7857, 51-55 [arXiv:2002.12347].
[8] N. Husung, P. Marquard and R. Sommer, Eur. Phys. J. C **80** (2020) no.3, 200 [arXiv:1912.08498].
[9] P. Boyle, F. Erben, *et al.* [arXiv:2406.19193].
[10] C. Lehner and A. S. Meyer, Phys. Rev. D **101** (2020), 074515 [arXiv:2003.04177].
[11] G. Wang *et al.* [chiQCD], Phys. Rev. D **107** (2023) no.3, 034513 [arXiv:2204.01280].
[12] C. Aubin, T. Blum, M. Golterman and S. Peris, Phys. Rev. D **106** (2022) no.5, 054503 [arXiv:2204.12256].
[13] M. Cè, A. Gérardin, *et al.* Phys. Rev. D **106** (2022) no.11, 114502 [arXiv:2206.06582].
[14] C. Alexandrou *et al.* [Extended Twisted Mass], Phys. Rev. D **107** (2023) no.7, 074506 [arXiv:2206.15084].
[15] A. Bazavov *et al.* [Fermilab Lattice, HPQCD, and MILC], Phys. Rev. D **107** (2023) no.11, 114514 [arXiv:2301.08274].
[16] T. Blum *et al.* [RBC and UKQCD], Phys. Rev. D **108** (2023) no.5, 054507 [arXiv:2301.08696].
[17] G. Benton, D. Boito, M. Golterman, A. Keshavarzi, K. Maltman and S. Peris, Phys. Rev. Lett. **131** (2023) no.25, 251803 [arXiv:2306.16808].
[18] M. Davier, A. Hoecker, A. M. Lutz, B. Malaescu and Z. Zhang, Eur. Phys. J. C **84** (2024), 721 [arXiv:2312.02053].
[19] B. Aubert *et al.* [BaBar], Phys. Rev. Lett. **103** (2009), 231801 [arXiv:0908.3589].
[20] J. P. Lees *et al.* [BaBar], Phys. Rev. D **86** (2012), 032013 [arXiv:1205.2228].
[21] F. Ambrosino *et al.* [KLOE], Phys. Lett. B **670** (2009), 285-291 [arXiv:0809.3950].
[22] F. Ambrosino *et al.* [KLOE], Phys. Lett. B **700** (2011), 102-110 [arXiv:1006.5313].
[23] D. Babusci *et al.* [KLOE], Phys. Lett. B **720** (2013), 336-343 [arXiv:1212.4524].
[24] A. Anastasi *et al.* [KLOE-2], JHEP **03** (2018), 173 [arXiv:1711.03085].
[25] F. V. Ignatov *et al.* [CMD-3], Phys. Rev. D **109** (2024) no.11, 112002 [arXiv:2302.08834].
[26] M. Davier, A. Hoecker, *et al.* Eur. Phys. J. C **66** (2010), 127-136 [arXiv:0906.5443].
[27] M. Davier, A. Höcker, B. Malaescu, C. Z. Yuan and Z. Zhang, Eur. Phys. J. C **74** (2014) no.3, 2803 [arXiv:1312.1501].
[28] M. Davier, A. Hoecker, B. Malaescu and Z. Zhang, Eur. Phys. J. C **80** (2020) no.3, 241 [erratum: Eur. Phys. J. C **80** (2020) no.5, 410] [arXiv:1908.00921].
[29] M. Davier, A. Hoecker, B. Malaescu, C. Z. Yuan and Z. Zhang, Eur. Phys. J. C **66** (2010), 1-9 [arXiv:0908.4300].
[30] M. Davier, A. Hoecker, B. Malaescu and Z. Zhang, Eur. Phys. J. C **71** (2011), 1515 [erratum: Eur. Phys. J. C **72** (2012), 1874] [arXiv:1010.4180].
[31] M. Davier, A. Hoecker, B. Malaescu and Z. Zhang, Eur. Phys. J. C **77** (2017) no.12, 827 [arXiv:1706.09436].